Intra-neuronal alpha-synuclein deposition is related to cardiac noradrenergic deficiency and olfactory dysfunction in neurogenic orthostatic hypotension

Risa Isonaka
National Institute of Neurological Disorders and Stroke Division of Intramural Research
Patti Sullivan
National Institute of Neurological Disorders and Stroke Division of Intramural Research
Courtney Holmes
National Institute of Neurological Disorders and Stroke Division of Intramural Research
David S. Goldstein
goldsteind@ninds.nih.gov

National Institute of Neurological Disorders and Stroke Intramural Research Program
https://orcid.org/0000-0002-5709-9940

Research Article

Keywords: synuclein, fluorodopamine, olfactory, orthostatic hypotension, Lewy

Posted Date: March 1st, 2024

DOI: https://doi.org/10.21203/rs.3.rs-3988235/v1

Intra-neuronal alpha-synuclein deposition is related to cardiac noradrenergic deficiency and olfactory dysfunction in neurogenic orthostatic hypotension

Risa Isonaka[1], Patti Sullivan[1], Courtney Holmes[1], David S. Goldstein[1]

[1]*Autonomic Medicine Section, Clinical Neurosciences Program, Division of Intramural Research, National Institute of Neurological Disorders and Stroke, National Institutes of Health, Bethesda, MD*

Short title: Lewy Body nOH

Keywords: synuclein; fluorodopamine; olfactory; orthostatic hypotension; Lewy

Corresponding author: David S. Goldstein, MD PhD, *Autonomic Medicine Section*, NINDS, NIH, 10 Center Drive MSC-1620, Building 10 Room 8N260, Bethesda, MD 20892-1620 USA. Phone: 301-496-2103. Fax: 301-402-0180. iPhone: 301-675-1110. e-mail: goldsteind@ninds.nih.gov. ORCID ID=0000-0002-5709-9940.

Counts: Abstract words: 250. Manuscript words: 3,276. Figures: 7. Tables: 0. Words in Title: 21. References: 58. Supplementary Data Workbooks: 1. Supplementary Tables: 1.

FINANCIAL SUPPORT: Division of Intramural Research, NINDS, NIH.

CONFLICTS OF INTEREST: The authors have no conflicts of interest to disclose.

ABSTRACT

Purpose: Neurogenic orthostatic hypotension (nOH) results from deficient reflexive delivery of norepinephrine to cardiovascular receptors in response to decreased cardiac venous return. Lewy body (LB) forms of nOH entail low ^{18}F-dopamine-derived radioactivity (a measure of cardiac noradrenergic deficiency), olfactory dysfunction by the University of Pennsylvania Smell Identification Test (UPSIT), and increased deposition of alpha-synuclein (α-syn) in dermal sympathetic noradrenergic nerves by the α-syn-tyrosine hydroxylase (TH) colocalization index. This observational, cross-sectional study explored whether combinations of these biomarkers specifically identify LB forms of nOH.

Methods: Clinical laboratory data were reviewed from patients referred for evaluation at the National Institutes of Health for chronic autonomic failure between 2011 and 2023. The cutoff value for low myocardial ^{18}F-dopamine-derived radioactivity was 6,000 nCi-kg/cc-mCi, for olfactory dysfunction an UPSIT score ≤ 28, and for an increased α-syn-TH colocalization index ≥ 1.57.

Results: A total of 44 patients (31 LB, 13 non-LB nOH) had data for all 3 biomarkers. Compared to the non-LB group, the LB nOH group had low myocardial ^{18}F-dopamine-derived radioactivity, low UPSIT scores, and high α-syn-TH colocalization indexes ($p<0.0001$ each). Combining the 3 biomarkers completely separated the groups. Cluster analysis identified 2 distinct groups ($p<0.0001$) independently of the clinical diagnosis, 1 cluster corresponding exactly to LB nOH.

Conclusion: LB forms of nOH feature cardiac noradrenergic deficiency, olfactory dysfunction, and increased α-syn-TH colocalization in skin biopsies. Combining the data for these variables efficiently separates LB from non-LB nOH. Independently of the clinical diagnosis, this biomarker triad identifies a pathophysiologically distinct cluster of nOH patients.

INTRODUCTION

Orthostatic hypotension is considered to be neurogenic (nOH) when the patient has persistent, consistent OH, there is no identified secondary cause, and there is evidence of decreased ability to maintain blood pressure reflexively in response to decreased venous return to the heart [11]. nOH occurs in a substantial minority of patients with Parkinson's disease (PD) [56], most patients with multiple system atrophy (MSA), and all patients with pure autonomic failure (PAF). These diseases are synucleinopathies, involving intra-cytoplasmic deposition of the protein alpha-synuclein (α-syn). In Lewy body (LB) forms of synucleinopathy the protein typically is deposited in neurons, whereas in MSA the deposits are in glial cytoplasmic inclusions [57]. Clinically diagnosed PAF can phenoconvert to PD, MSA, or dementia with Lewy bodies (DLB) [36].

It is difficult to distinguish LB from non-LB forms of nOH by clinical examination alone. There has long been interest in identifying biomarkers that might make this distinction. The first such biomarker to be described was cardiac sympathetic neuroimaging by ^{18}F-dopamine positron emission tomography (PET) [19]. ^{18}F-Dopamine is especially powerful for separating PD+OH from the parkinsonian form of MSA, as virtually all patients with PD+OH have severely decreased ^{18}F-dopamine-derived radioactivity, whereas most patients with MSA have normal radioactivity [43].

Patients with LB forms of nOH often have olfactory dysfunction, based on scores on the University of Pennsylvania Smell Identification Test (UPSIT), whereas in MSA olfaction usually is normal or only mildly or moderately decreased [12, 27]. Moreover, across synucleinopathy patients olfactory dysfunction is related to neuroimaging evidence of cardiac noradrenergic deficiency, both by ^{18}F-dopamine PET [18] and ^{123}I-metaiodobenzylguanidine (^{123}I-MIBG) single photon emission computed tomography (SPECT) [41].

Neither cardiac sympathetic neuroimaging nor olfactory testing directly identifies synucleinopathy. Until relatively recently, confirming the occurrence of a LB disease required post-mortem neurohistopathology. Over about the past decade, however, evidence has accrued

for increased deposition of native or S129 phosphorylated α-syn in sympathetic noradrenergic nerve fibers in skin biopsies in PD, PAF, and DLB and not in MSA [4, 6, 32]. For separating LB from non-LB forms of nOH, quantification of an α-syn-tyrosine hydroxylase (TH) colocalization index has been validated by post-mortem analyses of sympathetic ganglion tissue [32].

Previous studies have not included concurrent measurements of cardiac sympathetic innervation, olfactory function, and α-syn-TH colocalization in patients with nOH. In this study we asked whether these biomarkers in combination can distinguish LB from non-LB forms of nOH. We also addressed the converse—whether the biomarker phenotypic pattern identifies two pathophysiologically distinct groups of nOH regardless of the clinical diagnosis.

Finally, although long-term trends in cardiac sympathetic innervation have been described [40], those in olfactory function and α-syn-TH colocalization have not. We therefore also analyzed longitudinal follow-up data for these measures from subgroups of study participants who underwent serial evauations at the National Institutes of Health (NIH) Clinical Center.

METHODS

Study Subjects

All the participants in this observational, cross-sectional study gave written informed consent before any research procedures were done. The protocols were approved by the Institutional Review Board (IRB) of the National Institute of Neurological Disorders and Stroke (NINDS) or the IRB of the NIH. All the patients had been referred for evaluation by the Autonomic Medicine Section (AMS, formerly Clinical Neurocardiology Section) of the Division of Intramural Research of the NINDS at the NIH Clinical Center. Clinical laboratory data were reviewed from all patients referred for evaluation by the AMS at the NIH between 2011 and 2023.

Neurogenic orthostatic hypotension

The presence or absence of nOH was determined based on beat-to-beat blood pressure responses to the Valsalva maneuver or orthostatic fractional increments in plasma norepinephrine levels [23, 29].

PAF, PD+OH, MSA, and other forms of nOH—autoimmune autonomic ganglionopathy (AAG), autoimmunity-associated autonomic failure with sympathetic denervation, AAD) were diagnosed based on previously published consensus statements [11, 14, 15, 35], case reports [20, 22, 24], and post-mortem data when available [33, 34]. We also used the UK Brain Bank criteria for PD [30], with the following exception. According to the UK Brain Bank criteria, early, prominent autonomic involvement excludes a diagnosis of PD. Findings by our group [16, 22, 25] and others [47] that OH can occur in preclinical PD question this statement.

^{18}F-Dopamine positron emission tomography

^{18}F-dopamine PET was carried out as described previously [18]. Briefly, 1 mCi of the tracer was injected intravenously over 3 minutes. The radioactivity concentration in the interventricular septum was averaged in the 5-minute dynamic frame beginning about 5 minutes after initiation of the injection (midpoint about 8 minutes). The decay-corrected radioactivity concentration, in nCi/cc, was adjusted for the administered dose per kg body mass and expressed in units of nCi-

kg/cc-mCi. A cutoff value of 6,000 nCi-kg/cc-mCi was used to define low ^{18}F-dopamine-derived radioactivity [25].

University of Pennsylvania Smell Identification Test

The 40-item UPSIT was administered according to instructions [8]. The raw score was not adjusted for age or sex. A cutoff value of 28 was chosen, corresponding to moderately severe olfactory dysfunction.

Skin biopsies for immunofluorescence confocal microscopy

The location of the skin biopsies was the C2 region of the nape of the neck. Three-mm diameter skin punch biopsy samples were placed in Zamboni fixative solution and kept at 4 °C for 18-20 hours, washed with Sorenson's phosphate buffer (133 mM, pH 7.6), and placed in 20% glycerol for cryoprotection. Samples were embedded in optimum cutting temperature compound, frozen, sliced into 8-10 μm thick sections (Histoserv, Germantown, MD), and kept frozen at -80 °C until thawed for assay.

The primary antibodies used were as follows: rabbit anti-tyrosine hydroxylase (TH) (1:1000; Pel-Freez Biologicals, Rogers, AR), mouse IgG_1 monoclonal anti-α-synuclein (α-syn) (1:1000; Santa Cruz Biotechnology, Santa Cruz, CA), and mouse IgG_{2a} monoclonal anti-alpha-smooth muscle actin (SMA) (1:400; Santa Cruz Biotechnology). For the detection of S129 phosphorylated α-syn, a recombinant monoclonal rabbit antibody was used (Abcam Inc., Waltham, MA). When this antibody was employed, the primary antibody to TH was switched to chicken anti-TH (1:500; Abcam Inc.). The primary immunoreactions were visualized with the following secondary antibodies: Alexa 488-conjugated anti-mouse IgG_1 for α-syn, Alexa 555-conjugated anti-rabbit for TH, and when detecting phosphorylated α-syn Alexa 488-conjugated anti-rabbit. For chicken anti-TH, Alexa 555-conjugated anti-chicken was utilized. Additionally, Alexa 647-conjugated anti-mouse IgG_{2a} was used for SMA (all from Thermo Scientific, Inc, Rockford, IL).

Follow-up data

Although most of this study was cross-sectional, there was a longitudinal aspect. Subgroups of the study participants had serial data for cardiac ^{18}F-dopamine-derived radioactivity, UPSIT scores, and α-syn-TH colocalization indexes during follow-up evaluations at the NIH Clinical Center.

Avoidance of biases

The confocal microscopic imaging and subsequent image analyses were conducted at the NIH by personnel who were strictly blinded as to the diagnostic group until the data were tabulated. The clinical team was also blinded as to the imaging data until the data were tabulated. Personnel analyzing PET images were blinded as to both the clinical laboratory results and skin biopsy data.

Data Analysis and Statistics

α-Syn-TH colocalization in entire images was analyzed using Fiji software, with background subtraction as described previously [32]. α-Syn-TH colocalization indexes were calculated in the following steps: (1) normalized mean deviation product (nMDP) values from -1.0 to +1.0 were tabulated; (2) counts corresponding to nMDP values from 0.3 to 1.0 were summed; (3) 0.1 was added, so that the sum of the counts was greater than zero; and (4) the log of the number from step (3) was calculated.

GraphPad Prism 9 for Mac (GraphPad Software, Boston, MA) was used for most of the statistical analyses and graphics. Mean values in the LB and Non-LB nOH groups were compared by independent-means t tests. XY 3-D scatterplots were created to display individual values for the 3 biomarkers and for values across years of follow-up.

Fisher's exact test was used to compare the frequencies of abnormal biomarkers, alone or in combination, in the LB nOH and Non-LB nOH groups.

Pearson correlation coefficients were calculated for phosphorylated α-syn-TH colocalization indexes vs. native α-syn-TH colocalization indexes.

We performed a cluster analysis on the data for the 3 biomarkers using the k-means algorithm, as implemented in the KMeans function from the sklearn library in Python 3.12.1

(https://scikit-learn.org/). There were three general reasons for using KMeans. First, unlike simple correlation matrices, clustering algorithms like KMeans can discern and adapt to non-linear relationships and dependencies in the data, offering resilience against outliers and complex dynamics. Second, while multicollinearity can confound coefficient estimates in regression models, KMeans remains unaffected. This attribute stems from the algorithm's focus on the spatial structure of the data rather than the interdependencies among variables. Third, physiological processes often operate in discrete states of equilibrium. Correlations that are apparent within individual states may not extend across states. KMeans clustering effectively delineates these states, revealing distinct patterns and guiding in-depth analysis into the underlying physiological phenomena.

The KMeans algorithm partitions the dataset into a user-defined number of clusters. Unlike methods that deduce the optimal number of clusters through intrinsic dataset properties, KMeans necessitates a pre-specified cluster count. For our analysis, we selected a bifurcation approach, hypothesizing the data could be categorically divided into 2 distinct clusters. The assignment of data points to clusters is achieved by minimizing the total squared Euclidean distance between each point and the centroid of its assigned cluster. This iterative optimization process refines the centroids and the cluster memberships until the most compact and distinct grouping is attained. Given the disparate scales of variables in our dataset, standardization is pivotal. By standardizing, we ensured that each feature contributed equally to the analysis, akin to calibrating axes in a graph for uniform scale and comparability. This structured approach to clustering facilitated a nuanced exploration of the data, uncovering patterns and relationships that might elude traditional analytical methods.

To evaluate the probability of the observed clustering occurring by chance, we considered K successes in n draws, without replacement, from a finite population of N that contains exactly K objects with that feature. The formula for this is: $P(X = k) = (K,k)*(N-K,n-k) / (N,n)$, which can be simplified to $P(X=k) = (K,k)/(N,n)$, where the notation (A,B) is the binomial coefficient,

204 which stands for the number of ways that we can draw B draws from a population of A without
205 regard to the order, which is A!/(B!(B-a)!).
206

RESULTS

The dataset for this study corresponded to evaluations of 44 patients who had ^{18}F-dopamine PET, UPSIT scores, and skin biopsies analyzed for α-syn-TH colocalization indexes. In patients with biomarker values over multiple visits, for statistical analyses the values were averaged across the visits. All 3 biomarkers separated the LB from the non-LB forms of nOH (Fig. 1), although there were overlaps in the distributions.

Trends over years

For all 3 biomarkers, abnormal values in the subgroup of LB nOH patients with follow-up data persisted over years (Fig. 2); normal values in the small subgroup of non-LB nOH patients also persisted. In both subgroups there were no trends over years in values for any of the biomarkers.

Biomarker combinations

Combining cardiac ^{18}F-dopamine-derived radioactivity with UPSIT scores efficiently separated the LB from the non-LB patients (Fig. 3A). Among 31 LB nOH patients with data about ^{18}F-dopamine-derived radioactivity and UPSIT scores, 28 (90%) had abnormal values for both biomarkers. In contrast, none of 13 non-LB nOH patients (0%) had abnormal values for both biomarkers ($p<0.0001$ by Fisher's exact test). For separating the LB and non-LB nOH groups the sensitivity of this biomarker combination therefore was 90% at a specificity of 100%.

When cardiac ^{18}F-dopamine-derived radioactivity was expressed vs. α-syn-TH colocalization indexes, there was also good separation of the LB nOH from the non-LB nOH group (Fig. 3B). Among 31 patients in the LB nOH group, 24 (77%) had abnormal values for both biomarkers, while 0 of 13 (0%) in the non-LB nOH group had this combination ($p<0.0001$, sensitivity 77%, specificity 100%).

When UPSIT scores were related to α-syn-TH colocalization indexes, again there was good separation of the LB and non-LB nOH groups (Fig. 3C). Among the 31 patients in the LB group, 24 (77%) had abnormal values for both biomarkers, while 0 of 13 (0%) in the non-LB group had this combination, ($p<0.0001$, sensitivity 77%, specificity 100%).

For none of the 2-biomarker combinations was the separation perfect between the LB nOH and non-LB nOH groups. When all 3 parameters were considered together, however, there was complete separation of the LB and non-LB groups (See the 3-D scatterplot in Fig. 4).

Phosphorylated α-synuclein

For distinguishing the LB from the non-LB nOH groups the data for S129 phosphorylated α-syn-TH colocalization indexes were less robust than for native α-syn-TH colocalization indexes (Fig. 5A). Across 27 pairs of data for phosphorylated vs. native α-syn-TH colocalization indexes, the Pearson correlation coefficient was 0.59 ($p=0.012$) (Fig. 5B). Individual values for phosphorylated α-syn-TH colocalization indexes were unrelated to ^{18}F-dopamine-derived radioactivity (Fig. 5C) or to UPSIT scores (Fig. 5D).

Cluster analysis

The hypothesis underlying the cluster analysis was that the combined data for the 3 biomarkers form 2 distinct clusters. Supplementary Table 1 shows the cluster values, and the green diamonds in the 3-D scatterplot in Fig. 6 show the centroids for the 2 clusters. To evaluate the probability of the observed clustering occurring by chance, $K = k = n = 31$ patients in group 1, and $N = 44$. $P(X = 31) = (31,31)*(44-31,0)/(44,31)$. Since (31,31) and (13,0) simplify to 1, $P(X=31) = 1/(44,31)$, the value of $1/(44,31)$ was approximately $1.9 * 10^{-11}$, indicating indicating an extremely small likelihood that the observed clustering occurred by chance.

All the data in cluster 1 corresponded to patients diagnosed with a LB form of nOH, as demonstrated by the 3-D scatterplots in Supplementary Table 1 and comparison of Fig. 6 with Fig. 4.

DISCUSSION

In this study we obtained evidence that LB forms of nOH feature low myocardial ^{18}F-dopamine-derived radioactivity, low UPSIT scores, and elevated α-syn-TH colocalization indexes in skin biopsies compared to non-LB forms of nOH. All 3 biomarkers separated the groups, although the separations were imperfect. Combining the 3 biomarkers completely distinguished the groups. Conversely, cluster analysis performed on the biomarkers data independently of the clinical diagnosis identified 2 distinct clusters, with 1 of the clusters corresponding exactly to the group with a LB form of nOH.

The abnormalities of cardiac sympathetic innervation, olfaction, and α-syn deposition in sympathetic noradrenergic nerves persisted during follow-up in subgroups of LB nOH and non-LB nOH patients, without upward or downward trends. These findings suggest that the observed biomarker abnormalities were enduring traits. The study was not designed to ascertain when the abnormalities began with respect to the onset of nOH. There are no published studies directly on this key topic. It has been noted that rapid eye movement behavior disorder (RBD), which entails a high risk of development of a central synucleinopathy [52], is associated with OH [51, 53], abnormal cardiac sympathetic neuroimaging [37, 38], olfactory dysfunction [10, 54], and deposition of S129 phosphorylated α-syn in sympathetic noradrenergically innervated skin constituents [1, 5]; however, the timing of onset of these abnormalities with respect to RBD is poorly understood.

Because the UPSIT is effective, simple, inexpensive, widely available, and safe, we think this test (or an analogous test in non-English speakers) should be done in all patients with nOH. In essence this is an objective, quantifiable assessment of the first cranial nerve. A previous publication noted that olfactory dysfunction in PAF was not worse than that in MSA [55], but other studies have found that odor identification is impaired in PAF and not in MSA [12, 27]. In dementia, anosmia is found in DLB and not in Alzheimer's disease [45] and is common in Alzheimer's disease that is combined with LB pathology [50]. In patients with RBD the occurrence of olfactory dysfunction predicts early transition to a central LB disease [44].

283 The present results support our previous findings associating α-syn-TH colocalization with
284 both sporadic and familial LB diseases [31, 32, 34, 42]. Beginning with the publication by
285 Dabby et al. in 2006 [3] most reports on α-syn deposition in skin biopsies from patients with
286 synucleinopathies have been based on immunostaining for the pan-axonal marker protein gene
287 product (PGP) 9.5 [7, 46, 48, 58]. PGP 9.5 does not separate sensory from autonomic neurons
288 and among autonomic neurons does not identify sympathetic noradrenergic fibers specifically.
289 Indeed, PGP 9.5 may not even be completely specific for neuronal elements [2, 13].
290 For separating LB from non-LB forms of nOH, we found that α-syn-TH colocalization
291 indexes based on an antibody to native α-syn were superior to those based on an antibody to α-
292 syn phosphorylated at the 129S position. Although the LB nOH group had a higher mean
293 colocalization index based on 129S phosphorylated α-syn, and individual values for
294 colocalization indexes by the 2 assay methods were positively correlated, the α-syn-TH
295 colocalization indexes based on 129S phosphorylated α-syn were unrelated to cardiac ^{18}F-
296 dopamine-derived radioactivity and to UPSIT scores, whereas indexes based on native α-syn
297 were correlated with values for both biomarkers. It is possible that the antibody used for 129S
298 phosphorylated α-syn cross-reacted with other proteins. Alternatively, since the colocalization
299 method measures the extent of pixel-by-pixel correlations between α-syn and TH signals, if
300 129S phosphorylated α-syn were present outside catecholaminergic nerve fibers to an
301 appreciable extent, α-syn-TH colocalization indexes could be normal.
302 The present results confirm that ^{18}F-dopamine PET can identify LB forms of nOH [19, 21,
303 43]. Moreover, a recent prospective, longitudinal study showed that cardiac noradrenergic
304 deficiency revealed by ^{18}F-dopamine PET identifies preclinical central LB diseases in at-risk
305 individuals [25].
306 The results of this study seem sufficiently robust for us to propose extending on our
307 previously published algorithm for clinical laboratory evaluation of nOH [28]. In the 4-step
308 algorithm depicted in Fig. 7, olfactory function is assessed by the UPSIT. OH is determined to be
309 neurogenic based on the BP pattern associated with the Valsalva maneuver or the orthostatic

fractional increase in plasma norepinephrine. (It should be noted that the ΔHR/ΔBP ratio during tilt table testing is specific but insensitive for detecting nOH [17, 49]). Skin biopsies are assayed for immunoreactive α-syn and TH to calculate the α-syn-TH colocalization index. ^{18}F-Dopamine PET is reserved for unusual, difficult differential diagnostic cases or to optimize diagnostic enrichment in experimental therapeutic trials targeting LB forms of nOH. Each sequential step in Fig. 7 entails greater diagnostic accuracy at the costs of greater expense, risk, and practical limitations.

The biomarker triad of cardiac noradrenergic deficiency, olfactory dysfunction, and increased α-syn-TH colocalization indexes separated nOH into 2 distinct clusters, independently of the clinical diagnostic assignment. The p value for such clustering occurring by chance alone was about 2×10^{-11}, which is to say very close to zero. Importantly, 1 of the 2 clusters corresponded exactly to LB nOH. The present biomarkers data therefore support a phenotypic classification of nOH (LB vs. Non-LB nOH), which could prove valuable for diagnostic enrichment in experimental therapeutic trials.

Limitations

^{18}F-Dopamine PET is only available at the NIH Clinical Center. We hope that the present results will induce other institutions to apply for an IND so that this powerful technology is more widely used. Although ^{123}I-MIBG SPECT is available at most centers, insurance carriers in the United States do not cover cardiac ^{123}I-MIBG scanning in the diagnostic evaluation of LB diseases. We have commented about this deficiency for many years [9, 26, 39]. The generalizability of the present results therefore is unknown.

Conclusions

The biomarker triad of cardiac noradrenergic deficiency, olfactory dysfunction, and increased α-syn-TH colocalization indexes efficiently separates LB from non-LB forms of nOH. Conversely, independently of the clinical diagnosis, this combination of biomarkers separates distributions of individual data from nOH patients into 2 distinct clusters, with 1 cluster

corresponding to LB nOH. The biomarkers data support a 4-step algorithm for a pathophysiological identification of LB nOH.

REFERENCES

1. Antelmi E, Pizza F, Donadio V, Filardi M, Sosero YL, Incensi A, Vandi S, Moresco M, Ferri R, Marelli S, Ferini-Strambi L, Liguori R, Plazzi G (2019) Biomarkers for REM sleep behavior disorder in idiopathic and narcoleptic patients. Ann Clin Transl Neurol 6:1872-1876
2. Campbell LK, Thomas JR, Lamps LW, Smoller BR, Folpe AL (2003) Protein gene product 9.5 (PGP 9.5) is not a specific marker of neural and nerve sheath tumors: an immunohistochemical study of 95 mesenchymal neoplasms. Mod Pathol 16:963-969
3. Dabby R, Djaldetti R, Shahmurov M, Treves TA, Gabai B, Melamed E, Sadeh M, Avinoach I (2006) Skin biopsy for assessment of autonomic denervation in Parkinson's disease. J. Neural Transm. 113:1169-1176
4. Donadio V (2019) Skin nerve alpha-synuclein deposits in Parkinson's disease and other synucleinopathies: a review. Clin. Auton. Res. 29:577-585
5. Donadio V, Doppler K, Incensi A, Kuzkina A, Janzen A, Mayer G, Volkmann J, Rizzo G, Antelmi E, Plazzi G, Sommer C, Liguori R, Oertel WH (2019) Abnormal alpha-synuclein deposits in skin nerves: intra- and inter-laboratory reproducibility. Eur. J. Neurol. 26:1245-1251
6. Donadio V, Incensi A, Cortelli P, Giannoccaro MP, Jaber MA, Baruzzi A, Liguori R (2013) Skin sympathetic fiber alpha-synuclein deposits: a potential biomarker for pure autonomic failure. Neurology 80:725-732
7. Doppler K, Brockmann K, Sedghi A, Wurster I, Volkmann J, Oertel WH, Sommer C (2018) Dermal Phospho-Alpha-Synuclein Deposition in Patients With Parkinson's Disease and Mutation of the Glucocerebrosidase Gene. Front Neurol 9:1094
8. Doty RL, Deems DA, Stellar S (1988) Olfactory dysfunction in parkinsonism: a general deficit unrelated to neurologic signs, disease stage, or disease duration. Neurology 38:1237-1244

9. Eisenhofer G, Pacak K, Goldstein DS, Chen C, Shulkin B (2000) 123I-MIBG scintigraphy of catecholamine systems: impediments to applications in clinical medicine. Eur J Nucl Med 27:611-612.

10. Fantini ML, Postuma RB, Montplaisir J, Ferini-Strambi L (2006) Olfactory deficit in idiopathic rapid eye movements sleep behavior disorder. Brain Res. Bull. 70:386-390

11. Freeman R, Wieling W, Axelrod FB, Benditt DG, Benarroch E, Biaggioni I, Cheshire WP, Chelimsky T, Cortelli P, Gibbons CH, Goldstein DS, Hainsworth R, Hilz MJ, Jacob G, Kaufmann H, Jordan J, Lipsitz LA, Levine BD, Low PA, Mathias C, Raj SR, Robertson D, Sandroni P, Schatz I, Schondorff R, Stewart JM, van Dijk JG (2011) Consensus statement on the definition of orthostatic hypotension, neurally mediated syncope and the postural tachycardia syndrome. Clin. Auton. Res. 21:69-72

12. Garland EM, Raj SR, Peltier AC, Robertson D, Biaggioni I (2011) A cross-sectional study contrasting olfactory function in autonomic disorders. Neurology 76:456-460

13. Gilbert J, Norris MD, Marshall GM, Haber M (1997) Low specificity of PGP9.5 expression for detection of micrometastatic neuroblastoma. Br J Cancer 75:1779-1781

14. Gilman S, Low P, Quinn N, Albanese A, Ben-Shlomo Y, Fowler C, Kaufmann H, Kockgether T, Lang A, Lantos P, Litvan I, Mathias C, Oliver E, Robertson D, Schatz I, Wenning G (1998) Consensus statement on the diagnosis of multiple system atrophy. Clin. Auton. Res. 8:359-362

15. Gilman S, Wenning GK, Low PA, Brooks DJ, Mathias CJ, Trojanowski JQ, Wood NW, Colosimo C, Durr A, Fowler CJ, Kaufmann H, Klockgether T, Lees A, Poewe W, Quinn N, Revesz T, Robertson D, Sandroni P, Seppi K, Vidailhet M (2008) Second consensus statement on the diagnosis of multiple system atrophy. Neurology 71:670-676

16. Goldstein DS (2006) Orthostatic hypotension as an early finding in Parkinson disease. Clin. Auton. Res. 16:46-64

17. Goldstein DS, Dill S, Sullivan P, Grabov E, Chittiboina P (2023) Baroreflex-sympathoneural without baroreflex-cardiovagal failure in neurogenic orthostatic hypotension. Clin Auton Res 33:205-208
18. Goldstein DS, Holmes C, Bentho O, Sato T, Moak J, Sharabi Y, Imrich R, Conant S, Eldadah BA (2008) Biomarkers to detect central dopamine deficiency and distinguish Parkinson disease from multiple system atrophy. Parkinsonism Relat. Disord. 14:600-607
19. Goldstein DS, Holmes C, Cannon RO, 3rd, Eisenhofer G, Kopin IJ (1997) Sympathetic cardioneuropathy in dysautonomias. N. Engl. J. Med. 336:696-702
20. Goldstein DS, Holmes C, Dendi R, Li ST, Brentzel S, Vernino S (2002) Pandysautonomia associated with impaired ganglionic neurotransmission and circulating antibody to the neuronal nicotinic receptor. Clin. Auton. Res. 12:281-285
21. Goldstein DS, Holmes C, Li ST, Bruce S, Metman LV, Cannon RO, 3rd (2000) Cardiac sympathetic denervation in Parkinson disease. Ann. Intern. Med. 133:338-347
22. Goldstein DS, Holmes C, Sewell L, Park MY, Sharabi Y (2012) Sympathetic noradrenergic before striatal dopaminergic denervation: relevance to Braak staging of synucleinopathy. Clin. Auton. Res. 22:57-61
23. Goldstein DS, Holmes C, Sharabi Y, Brentzel S, Eisenhofer G (2003) Plasma levels of catechols and metanephrines in neurogenic orthostatic hypotension. Neurology 60:1327-1332
24. Goldstein DS, Holmes C, Sullivan P, Donadio V, Isonaka R, Zhong E, Pourier B, Vernino S, Kopin IJ, Sharabi Y (2017) Autoimmunity-associated autonomic failure with sympathetic denervation. Clin. Auton. Res. 27:57-62
25. Goldstein DS, Holmes C, Sullivan P, Lopez G, Gelsomino J, Moore S, Isonaka R, Wu T, Sharabi Y (2024) Cardiac noradrenergic deficiency revealed by 18F-dopamine positron emission tomography identifies preclinical central Lewy body diseases. J Clin Invest 134
26. Goldstein DS, Orimo S (2009) Cardiac sympathetic neuroimaging: summary of the First International Symposium. Clin. Auton. Res. 19:133-136

27. Goldstein DS, Sewell L (2009) Olfactory dysfunction in pure autonomic failure: Implications for the pathogenesis of Lewy body diseases. Parkinsonism Relat. Disord. 15:516-520

28. Goldstein DS, Sharabi Y (2009) Neurogenic orthostatic hypotension: a pathophysiological approach. Circulation 119:139-146

29. Goldstein DS, Tack C (2000) Non-invasive detection of sympathetic neurocirculatory failure. Clin. Auton. Res. 10:285-291

30. Hughes AJ, Daniel SE, Kilford L, Lees AJ (1992) Accuracy of clinical diagnosis of idiopathic Parkinson's disease: a clinico-pathological study of 100 cases. J. Neurol. Neurosurg. Psychiatry 55:181-184

31. Isonaka R, Goldstein DS, Zhu W, Yoon E, Ehrlich D, Schindler AB, Kokkinis AD, Sabir MS, Scholz SW, Bandres-Ciga S, Blauwendraat C, Gonzalez-Alegre P, Lopez G, Sidransky E, Narendra DP (2021) alpha-Synuclein Deposition in Sympathetic Nerve Fibers in Genetic Forms of Parkinson's Disease. Mov Disord 36:2346-2357

32. Isonaka R, Rosenberg AZ, Sullivan P, Corrales A, Holmes C, Sharabi Y, Goldstein DS (2019) Alpha-Synuclein deposition within sympathetic noradrenergic neurons Is associated with myocardial noradrenergic deficiency in neurogenic orthostatic hypotension. Hypertension 73:910-918

33. Isonaka R, Sullivan P, Goldstein DS (2022) Pathophysiological significance of increased alpha-synuclein deposition in sympathetic nerves in Parkinson's disease: a post-mortem observational study. Transl Neurodegener 11:15

34. Isonaka R, Sullivan P, Jinsmaa Y, Corrales A, Goldstein DS (2018) Spectrum of abnormalities of sympathetic tyrosine hydroxylase and alpha-synuclein in chronic autonomic failure. Clin. Auton. Res. 28:223-230

35. Kaufmann H (1996) Consensus statement on the definition of orthostatic hypotension, pure autonomic failure and multiple system atrophy. Clin. Auton. Res. 6:125-126

442 36. Kaufmann H, Norcliffe-Kaufmann L, Palma JA, Biaggioni I, Low PA, Singer W, Goldstein
443 DS, Peltier AC, Shibao CA, Gibbons CH, Freeman R, Robertson D (2017) Natural history
444 of pure autonomic failure: A United States prospective cohort. Ann. Neurol. 81:287-297
445 37. Kim JS, Park HE, Oh YS, Lee SH, Park JW, Son BC, Lee KS (2016) Orthostatic
446 hypotension and cardiac sympathetic denervation in Parkinson disease patients with REM
447 sleep behavioral disorder. J. Neurol. Sci. 362:59-63
448 38. Knudsen K, Fedorova TD, Hansen AK, Sommerauer M, Otto M, Svendsen KB, Nahimi A,
449 Stokholm MG, Pavese N, Beier CP, Brooks DJ, Borghammer P (2018) In-vivo staging of
450 pathology in REM sleep behaviour disorder: a multimodality imaging case-control study.
451 Lancet Neurol. 17:618-628
452 39. Lamotte G, Goldstein DS (2022) What new can we learn from cardiac sympathetic
453 neuroimaging in synucleinopathies? Clin Auton Res 32:95-98
454 40. Lamotte G, Holmes C, Wu T, Goldstein DS (2019) Long-term trends in myocardial
455 sympathetic innervation and function in synucleinopathies. Parkinsonism Relat. Disord.
456 67:27-33
457 41. Lee PH, Yeo SH, Kim HJ, Youm HY (2006) Correlation between cardiac 123I-MIBG and
458 odor identification in patients with Parkinson's disease and multiple system atrophy. Mov.
459 Disord. 21:1975-1977
460 42. Lenka A, Isonaka R, Holmes C, Goldstein DS (2023) Cardiac (18)F-dopamine positron
461 emission tomography predicts the type of phenoconversion of pure autonomic failure. Clin
462 Auton Res 33:737-747
463 43. Lenka A, Lamotte G, Goldstein DS (2021) Cardiac (18)F-Dopamine PET Distinguishes PD
464 with Orthostatic Hypotension from Parkinsonian MSA. Mov Disord Clin Pract 8:582-586
465 44. Mahlknecht P, Iranzo A, Hogl B, Frauscher B, Muller C, Santamaria J, Tolosa E, Serradell
466 M, Mitterling T, Gschliesser V, Goebel G, Brugger F, Scherfler C, Poewe W, Seppi K,
467 Sleep Innsbruck Barcelona G (2015) Olfactory dysfunction predicts early transition to a
468 Lewy body disease in idiopathic RBD. Neurology 84:654-658

469 45. McShane RH, Nagy Z, Esiri MM, King E, Joachim C, Sullivan N, Smith AD (2001)
470 Anosmia in dementia is associated with Lewy bodies rather than Alzheimer's pathology. J.
471 Neurol. Neurosurg. Psychiatry. 70:739-743
472 46. Melli G, Vacchi E, Biemmi V, Galati S, Staedler C, Ambrosini R, Kaelin-Lang A (2018)
473 Cervical skin denervation associates with alpha-synuclein aggregates in Parkinson disease.
474 Ann Clin Transl Neurol 5:1394-1407
475 47. Milazzo V, Di Stefano C, Servo S, Zibetti M, Lopiano L, Maule S (2012) Neurogenic
476 orthostatic hypotension as the initial feature of Parkinson disease. Clin Auton Res 22:203-
477 206
478 48. Navarro-Otano J, Casanova-Molla J, Morales M, Valls-Sole J, Tolosa E (2015) Cutaneous
479 autonomic denervation in Parkinson's disease. J Neural Transm (Vienna) 122:1149-1155
480 49. Norcliffe-Kaufmann L, Kaufmann H, Palma JA, Shibao CA, Biaggioni I, Peltier AC,
481 Singer W, Low PA, Goldstein DS, Gibbons CH, Freeman R, Robertson D, Autonomic
482 Disorders C (2018) Orthostatic heart rate changes in patients with autonomic failure caused
483 by neurodegenerative synucleinopathies. Ann. Neurol. 83:522-531
484 50. Olichney JM, Murphy C, Hofstetter CR, Foster K, Hansen LA, Thal LJ, Katzman R (2005)
485 Anosmia is very common in the Lewy body variant of Alzheimer's disease. J.Neurol.
486 Neurosurg. Psychiatry 76:1342-1347
487 51. Postuma RB, Gagnon JF, Pelletier A, Montplaisir J (2013) Prodromal autonomic symptoms
488 and signs in Parkinson's disease and dementia with Lewy bodies. Mov. Disord. 28:597-604
489 52. Postuma RB, Iranzo A, Hogl B, Arnulf I, Ferini-Strambi L, Manni R, Miyamoto T, Oertel
490 W, Dauvilliers Y, Ju YE, Puligheddu M, Sonka K, Pelletier A, Santamaria J, Frauscher B,
491 Leu-Semenescu S, Zucconi M, Terzaghi M, Miyamoto M, Unger MM, Carlander B,
492 Fantini ML, Montplaisir JY (2015) Risk factors for neurodegeneration in idiopathic rapid
493 eye movement sleep behavior disorder: a multicenter study. Ann Neurol 77:830-839

494 53. Romenets SR, Gagnon JF, Latreille V, Panniset M, Chouinard S, Montplaisir J, Postuma
495 RB (2012) Rapid eye movement sleep behavior disorder and subtypes of Parkinson's
496 disease. Mov. Disord. 27:996-1003
497 54. Siderowf A, Jennings D, Eberly S, Oakes D, Hawkins KA, Ascherio A, Stern MB, Marek
498 K, Investigators P (2012) Impaired olfaction and other prodromal features in the Parkinson
499 At-Risk Syndrome Study. Mov. Disord. 27:406-412
500 55. Silveira-Moriyama L, Mathias C, Mason L, Best C, Quinn NP, Lees AJ (2009) Hyposmia
501 in pure autonomic failure. Neurology 72:1677-1681
502 56. Velseboer DC, de Haan RJ, Wieling W, Goldstein DS, de Bie RM (2011) Prevalence of
503 orthostatic hypotension in Parkinson's disease: a systematic review and meta-analysis.
504 Parkinsonism Relat. Disord. 17:724-729
505 57. Wakabayashi K, Yoshimoto M, Tsuji S, Takahashi H (1998) Alpha-synuclein
506 immunoreactivity in glial cytoplasmic inclusions in multiple system atrophy. Neurosci.
507 Lett. 249:180-182
508 58. Wang N, Garcia J, Freeman R, Gibbons CH (2020) Phosphorylated Alpha-Synuclein
509 Within Cutaneous Autonomic Nerves of Patients With Parkinson's Disease: The
510 Implications of Sample Thickness on Results. J Histochem Cytochem 68:669-678
511
512

ACKNOWLEDGEMENTS

The research reported here was supported (in part) by the research Division of Intramural Research, National Institutes of Health (NINDS). We thank Zvi B. Goldstein for his technical assistance with updating the 3-D scatter plots and for performing the cluster analysis.

AUTHOR CONTRIBUTIONS:

RI: Methods development, data acquisition, data analysis, manuscript editing

PS: Data acquisition, data analysis, manuscript editing

CH: Data acquisition, data analysis, manuscript editing

DG: Study concept, data analysis, manuscript writing

DATA DICTIONARY FOR SUPPLEMENTARY DATA WORKBOOK

Tab "Neck Ave. if >1 Row"

Cells highlighted in blue with bold text indicate patients with more than 1 dataset; mean data across visits are displayed.

N=subject number

Skin Bx ID #=skin biopsy identification number

AGE=patient age, in years (no data if more than 1 dataset)

SEX=patient sex

GROUP=diagnostic group (PAF=pure autonomic failure; PD+OH=Parkinson's disease with orthostatic hypotension; GBA=glucocerebrosidase mutation heterozygote; MSA=multiple system atrophy; MSA-P=parkinsonian form of multiple system atrophy; AAG=autoimmune autonomic ganglionopathy; AAD=autoimmunity-associated autonomic failure with sympathetic denervation)

GROUP FOR LB nOH ms=patient group, stratified in terms of Lewy body nOH or non-Lewy body nOH

Biopsy Site=body site of skin biopsy (nape of neck)

Colocalization Index=alpha-synuclein/tyrosine hydroxylase colocalization index

Phosphorylated Colocalization Index=phosphorylated alpha-synuclein/tyrosine hydroxylase colocalization index

UPSIT Score=University of Pennsylvania Smell Identification Test score (maximum=40)

18F-DA=^{18}F-dopamine-derived radioactivity in the interventricular septum (8' frame)

UPSIT Abnl. =abnormally low score on the University of Pennsylvania Smell Identification Test score (cutoff=28, abnormal=1, not abnormal=0)

Coloc. Abnl. =abnormally elevated alpha-synuclein/tyrosine hydroxylase colocalization index (cutoff=1.57, abnormal=1, not abnormal=0)

18FDA Abnl=abnormally low ^{18}F-dopamine-derived radioactivity (cutoff=6,000 nCi-kg/cc-mCi, abnormal=1, not abnormal=0)

UPSIT & Coloc. Abnl. =both UPSIT and alpha-synuclein/tyrosine hydroxylase colocalization index abnormal (1) or not both abnormal (0)

UPSIT & 18FDA Abnl. =both UPSIT and ^{18}F-dopamine-derived radioactivity abnormal (1) or not both abnormal (0)

18FDA & Coloc. Abnl. =both ^{18}F-dopamine-derived radioactivity and alpha-synuclein/tyrosine hydroxylase colocalization index abnormal (1) or not both abnormal (0)

All 3 Abnormal=^{18}F-dopamine-derived radioactivity, UPSIT score, and alpha-synuclein/tyrosine hydroxylase colocalization index all abnormal (1) or not all abnormal (0)

Tab "Neck Repeats ≥ 2 Years"

AGE=patient age, in years

SEX=patient sex

GROUP=diagnostic group (PAF=pure autonomic failure; PD+OH=Parkinson's disease with orthostatic hypotension; GBA=glucocerebrosidase mutation heterozygote; MSA=multiple system atrophy; MSA-P=parkinsonian form of multiple system atrophy; AAG=autoimmune autonomic ganglionopathy; AAD=autoimmunity-associated autonomic failure with sympathetic denervation)

GROUP FOR LB nOH ms=patient group, stratified in terms of Lewy body nOH or non-Lewy body nOH

Biopsy Site=body site of skin biopsy (nape of neck)

F/U Years=years since initial evaluation

Colocalization Index=alpha-synuclein/tyrosine hydroxylase colocalization index

UPSIT Score=University of Pennsylvania Smell Identification Test score (maximum=40)

18F-DA=^{18}F-dopamine-derived radioactivity in the interventricular septum (8' frame)

FIGURES AND FIGURE LEGENDS

Fig. 1: Individual values for (A) ^{18}F-dopamine- (^{18}F-DA)-derived radioactivity, (B) scores on the University of Pennsylvania Smell Identification Test (UPSIT), and (C) α-synuclein-tyrosine hydroxylase colocalization (Coloc.) indexes in groups with Lewy body (LB, red circles) and non-Lewy body (Non-LB, blue squares) forms of neurogenic orthostatic hypotension.

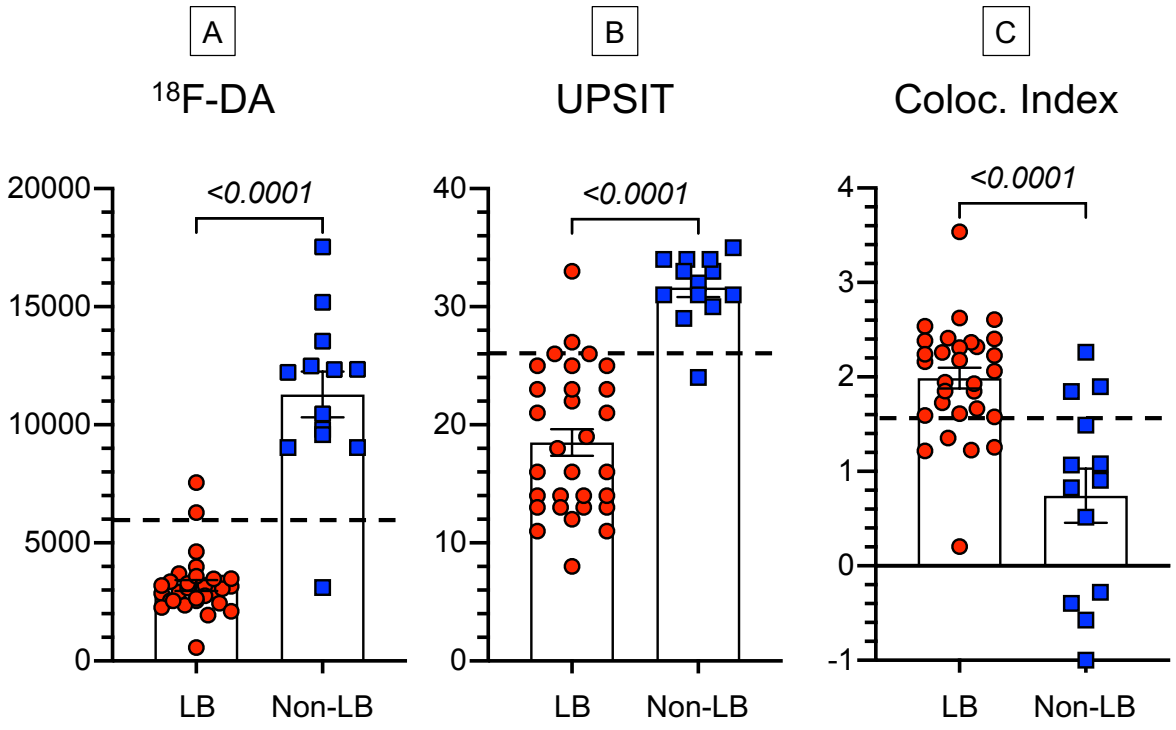

Mean ± SEM values are displayed. Numbers in italics are p values for independent-means t tests comparing the LB vs. non-LB groups. Dashed lines show cutoff values for ^{18}F-dopamine-derived radioactivity (normal >6,000 nCi-kg/cc-mCi), UPSIT scores (normal >28), and colocalization indexes (normal<1.57). All 3 biomarkers distinguished the LB from the Non-LB groups, but with overlaps in the data distributions.

Fig. 2: Individual values for (A) ^{18}F-dopamine- (^{18}F-DA)-derived radioactivity, (B) scores on the University of Pennsylvania Smell Identification Test (UPSIT), and (C) α-synuclein-tyrosine hydroxylase colocalization (Coloc.) indexes as a function of years of follow-up in patients with Lewy body (LB, red circles, solid lines) or non-Lewy body (Non-LB, blue squares, thin dashed lines) forms of neurogenic orthostatic hypotension.

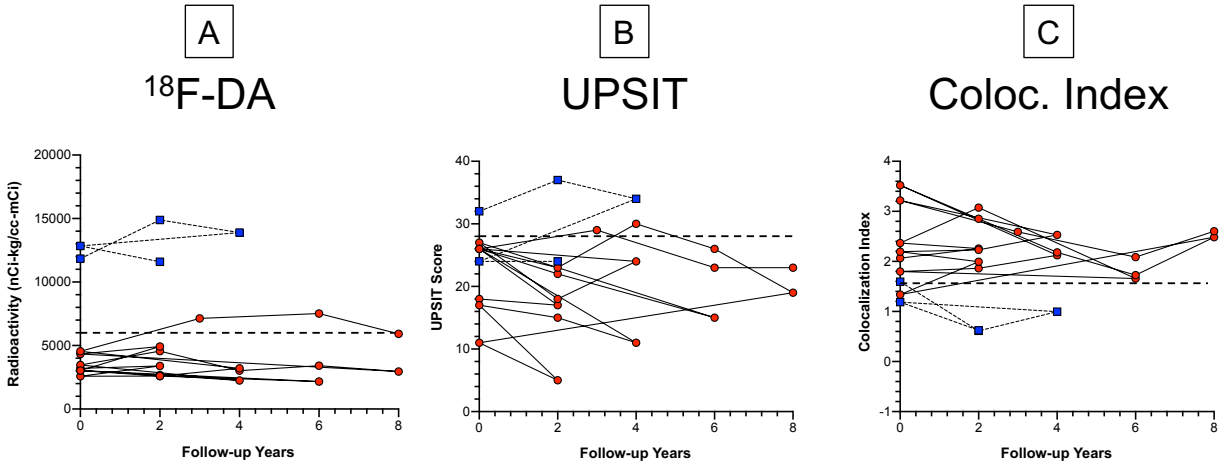

Thick dashed lines show cutoff values for ^{18}F-dopamine-derived radioactivity (normal >6,000 nCi-kg/cc-mCi), UPSIT scores (normal >28), and colocalization indexes (normal<1.57). For all 3 biomarkers, abnormal values in the LB nOH patients and normal values in the LB No OH patients persisted during follow-up.

Fig. 3: Combinations of 2 biomarkers: (A) UPSIT scores and cardiac ^{18}F-dopamine-derived radioactivity, (B) cardiac ^{18}F-dopamine-derived radioactivity and α-synuclein-tyrosine hydroxylase colocalization indexes, and (C) UPSIT scores and α-synuclein-tyrosine hydroxylase colocalization indices in groups with Lewy body (LB, red circles) or non-Lewy body (Non-LB, blue squares) forms of neurogenic orthostatic hypotension.

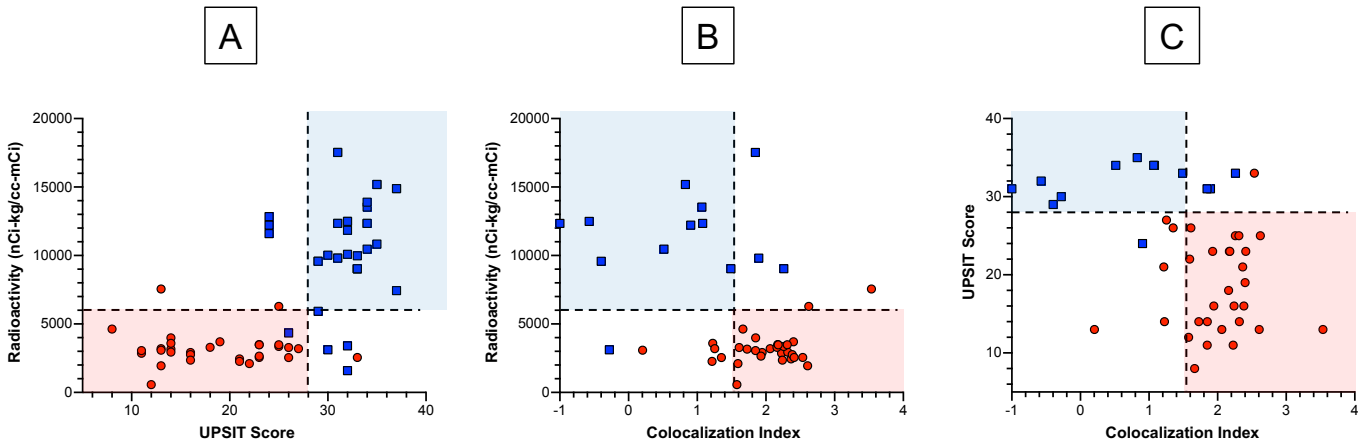

Dashed lines show cutoff values for ^{18}F-dopamine-derived radioactivity (normal >6,000 nCi-kg/cc-mCi), UPSIT scores (normal >28), and colocalization indexes (normal<1.57). For all 3 biomarker combinations there were distinct but imperfect separations between the LB and non-LB groups, as indicated by the pink and blue rectangles.

Fig. 4: 3-D scatter plot showing complete separation of Lewy body (LB, red circles) from non-LB forms of neurogenic orthostatic hypotension, based on cardiac ^{18}F-dopamine-derived radioactivity, scores on the University of Pennsylvania Smell Identification Test (UPSIT), and α-synuclein-tyrosine hydroxylase colocalization indexes.

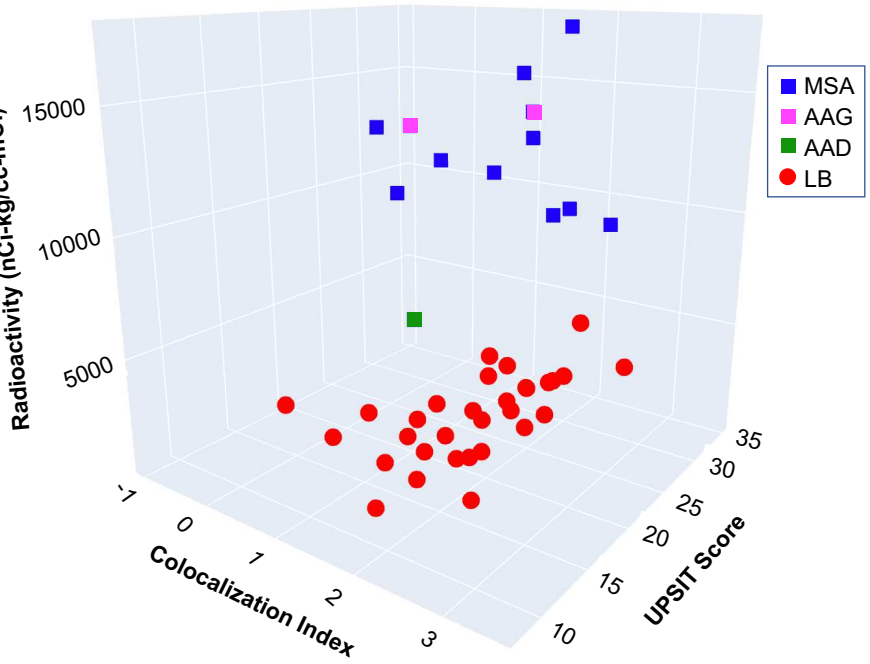

Blue squares correspond to patients with multiple system atrophy (MSA), magenta squares patients with autoimmune autonomic ganglionopathy (AAG), and green square a patient with autoimmunity-associated autonomic failure with sympathetic denervation (AAD).

Fig. 5: Phosphorylated α-synuclein (α-syn)-tyrosine hydroxylase (TH) colocalization indexes in Lewy body (LB, red) and non-Lewy body (Non-LB, blue) forms of neurogenic orthostatic hypotension (nOH).

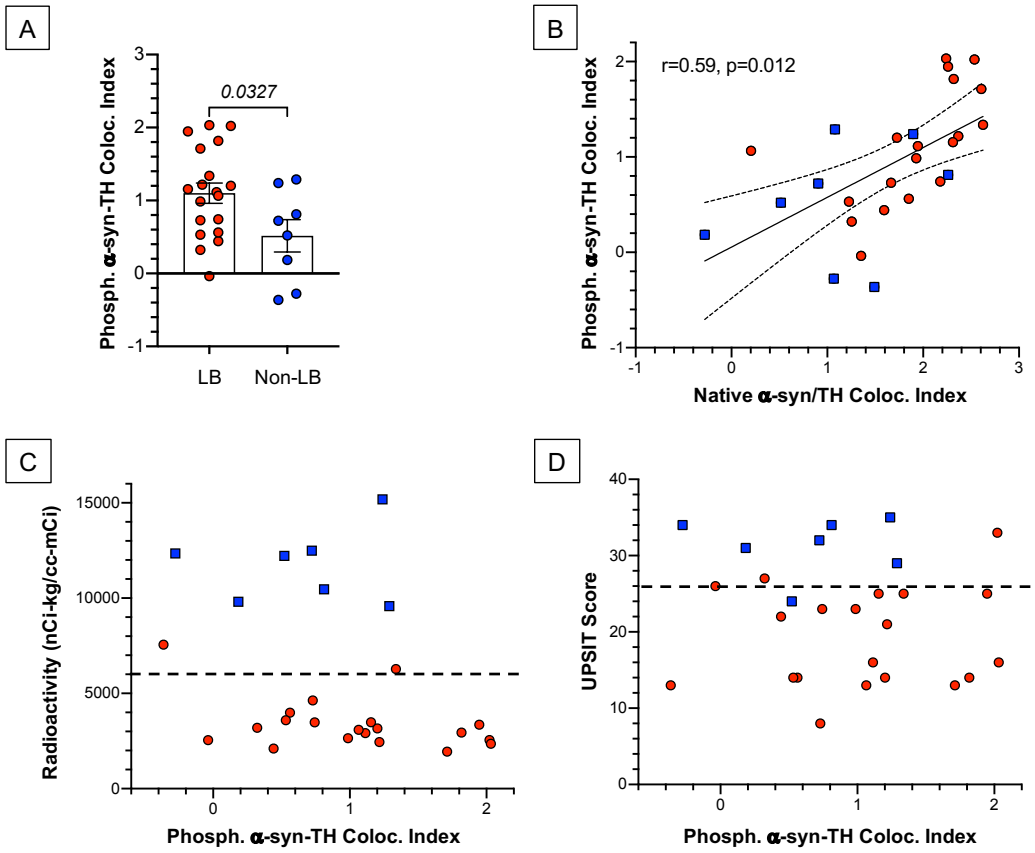

(A) Individual values for phosphorylated α-syn-TH colocalization indexes, with means and SEMs. Number in italics is the p value for the independent-means t-test comparing the LB vs. Non-LB groups. (B) Scatterplot of individual values for phosphorylated α-syn-TH colocalization indexes vs. native α-syn/TH colocalization indexes. The linear regression line of best fit across all subjects is shown with 95% confidence intervals. Also displayed are the Pearson correlation coefficient and p value. (C) Individual values for ^{18}F-dopamine-derived radioactivity vs. phosphorylated α-syn-TH colocalization indexes. The dashed line shows the radioactivity cutoff value. (D) Individual values for scores on the University of Pennsylvania Smell Identification Test (UPSIT) vs. phosphorylated α-syn-TH colocalization indexes. The dashed line shows the UPSIT cutoff value.

Fig. 6: Cluster analysis of data for cardiac ^{18}F-dopamine-derived radioactivity, scores on the University of Pennsylvania Smell Identification Test (UPSIT), and α-synuclein-tyrosine hydroxylase colocalization indexes without regard to clinical diagnosis in patients with neurogenic orthostatic hypotension (nOH). The green diamonds show the centroids of the 2 clusters.

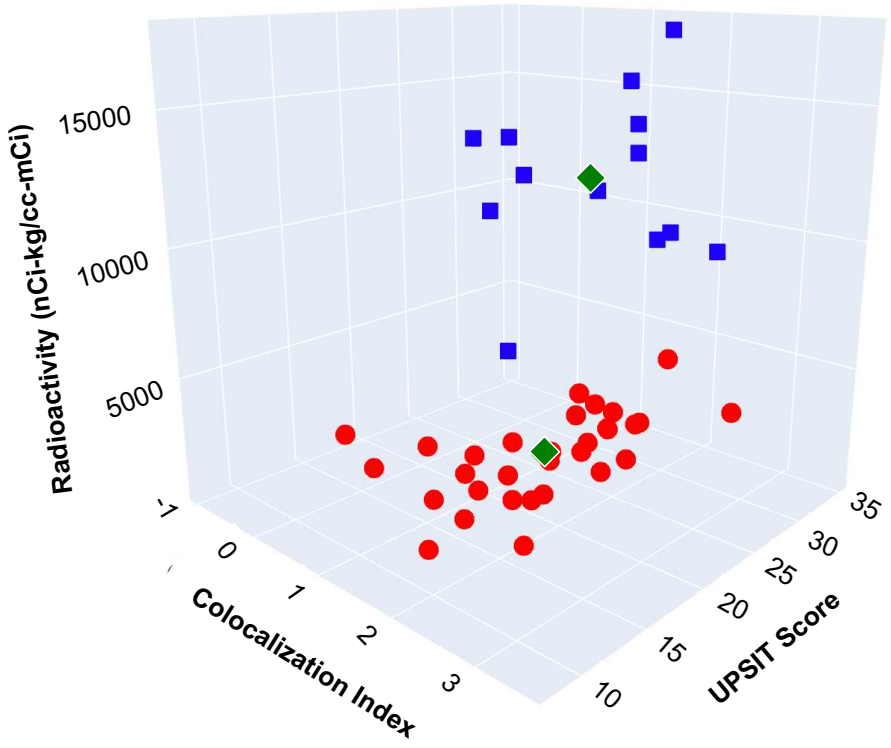

The data were divided into 2 clusters, with each cluster colored differently (cluster 1=red circles, cluster 2=blue squares). Comparison with Fig. 4 demonstrates that all the data in cluster 1 correspond to patients with LB forms of nOH. The Python code used for the cluster analysis is in Supplementary Table 1.

Fig. 7: Clinical laboratory algorithm for identifying Lewy body forms of neurogenic orthostatic hypotension (nOH)

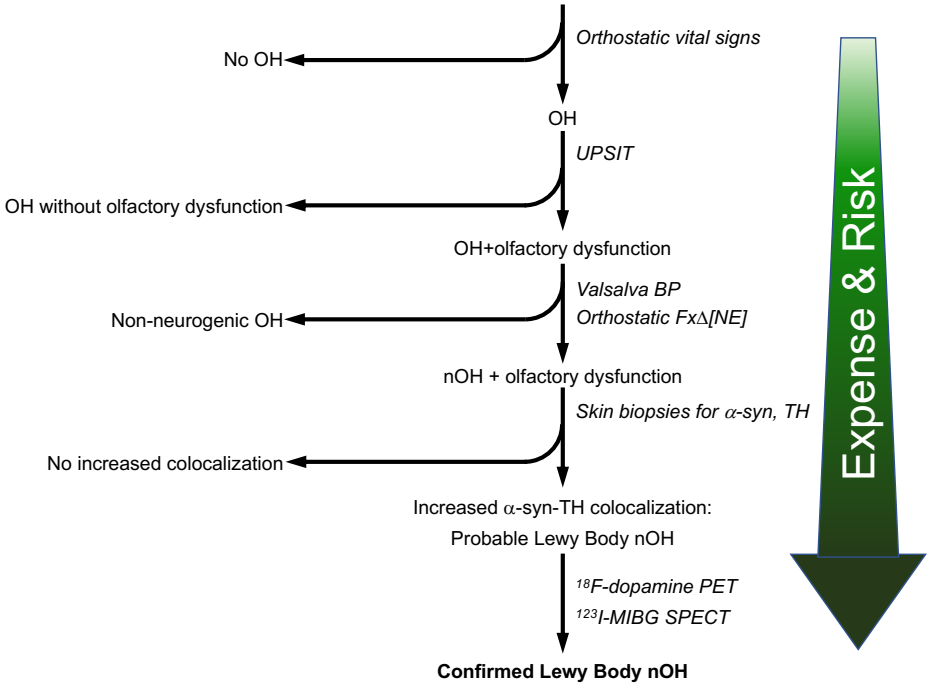

Each step entails greater diagnostic accuracy but with greater expense, risk, and practical limitations. Olfactory function is assessed by the University of Pennsylvania Smell Identification Test (UPSIT). OH is determined to be neurogenic based on the blood pressure pattern associated with the Valsalva maneuver (Valsalva BP) or on the orthostatic fractional increase in plasma norepinephrine (Orthostatic FxΔ[NE]). Skin biopsies are analyzed to calculate the alpha-synuclein (α-syn)-tyrosine hydroxylase (TH) colocalization index. Other abbreviations: ^{123}I-MIBG=^{123}I-metaiodobenzylguanidine; PET=positron emission tomography; SPECT=single photon emission computed tomography.

Supplementary Table 1: Python code and data for the 3-D scatterplots in Figs. 4 and 6.

```
import pandas as pd
from io import StringIO

import pandas as pd
import numpy as np
from sklearn.cluster import KMeans
import plotly.graph_objects as go
import plotly.express as px


# Data as a multi-line string
data_string = """
GROUP,Colocalization Index,UPSIT Score,Radioactivity (nCi-kg/cc-mCi),
LB nOH,2.4011,19,3699,
LB nOH,2.2273,11,2862,
LB nOH,1.7261,14,3157,
LB nOH,2.6068,13,1943,
LB nOH,2.3178,14,2943,
LB nOH,2.0617,13,3193,
LB nOH,1.9440,16,2913,
LB nOH,2.1715,23,3496,
LB nOH,2.1602,18,3294,
LB nOH,2.3661,21,2445,
LB nOH,1.5922,22,2102,
LB nOH,2.5353,33,2553,
LB nOH,0.2041,13,3085,
LB nOH,1.2157,21,2267,
LB nOH,2.3832,16,2759,
LB nOH,1.6103,26,3282,
LB nOH,1.5776,12,570,
LB nOH,1.8484,11,3055,
LB nOH,1.8494,14,3985,
LB nOH,2.4101,23,2549,
LB nOH,2.6239,25,6278,
LB nOH,2.2391,16,2354,
LB nOH,1.3525,26,2547,
LB nOH,2.2595,25,3356,
LB nOH,1.2251,14,3587,
LB nOH,1.2547,27,3194,
LB nOH,1.9276,23,2647,
LB nOH,2.3106,25,3481,
LB nOH,1.6652,8,4627,
LB nOH,2.1778,23,3476,
LB nOH,3.5364,13,7555,
```

```
Non-LB nOH,1.4900,33,9036,
Non-LB nOH,-0.5740,32,12489,
Non-LB nOH,0.9047,24,12215,
Non-LB nOH,0.5151,34,10462,
Non-LB nOH,2.2609,33,9036,
Non-LB nOH,0.8271,35,15182,
Non-LB nOH,1.8959,31,9810,
Non-LB nOH,-0.2795,30,3108,
Non-LB nOH,-0.3979,29,9581,
Non-LB nOH,1.0792,34,12341,
Non-LB nOH,1.0678,34,13539,
Non-LB nOH,1.8457,31,17527,
Non-LB nOH,-1.0000,31,12346,
"""
# Using StringIO to simulate a file object
data_io = StringIO(data_string)

# Create a DataFrame, using the first line as headers and ignore the trailing commas
df = pd.read_csv(data_io, sep=",")

# Display the DataFrame
df.head()
# Create a figure object
fig = go.Figure()

# Add LB nOH group in red circles
fig.add_trace(go.Scatter3d(
    x=df[df['GROUP'] == 'LB nOH']['Colocalization Index'],
    y=df[df['GROUP'] == 'LB nOH']['UPSIT Score'],
    z=df[df['GROUP'] == 'LB nOH']['Radioactivity (nCi-kg/cc-mCi)'],
    mode='markers',
    marker=dict(color='red', size=5, symbol='circle'),
    name='LB nOH',
    text=df[df['GROUP'] == 'LB nOH']['GROUP'],
    hoverinfo='text+x+y+z'
))

# Add non-LB nOH group in blue squares
fig.add_trace(go.Scatter3d(
    x=df[df['GROUP'] == 'Non-LB nOH']['Colocalization Index'],
    y=df[df['GROUP'] == 'Non-LB nOH']['UPSIT Score'],
    z=df[df['GROUP'] == 'Non-LB nOH']['Radioactivity (nCi-kg/cc-mCi)'],
    mode='markers',
    marker=dict(color='blue', size=5, symbol='square'),
    name='Non-LB nOH',
    text=df[df['GROUP'] == 'Non-LB nOH']['GROUP'],
```

```
    hoverinfo='text+x+y+z'
))

font_size = 10
# Update the layout to include the custom font settings
fig.update_layout(
    scene=dict(
        xaxis_title='Colocalization Index',
        yaxis_title='UPSIT Score',
        zaxis_title='Radioactivity (nCi-kg/cc-mCi)',
        xaxis=dict(title_font=dict(family="Arial", size=font_size, color="black"),
                tickfont=dict(family="Arial", size=font_size)),
        yaxis=dict(title_font=dict(family="Arial", size=font_size, color="black"),
                tickfont=dict(family="Arial", size=font_size)),
        zaxis=dict(title_font=dict(family="Arial", size=font_size, color="black"),
                tickfont=dict(family="Arial", size=font_size)),
    ),
    font=dict(family="Arial", size=font_size),
    width=800,  # Set the width of the plot
    height=800,  # Set the height of the plot
)

# Show the figure
fig.show()

from sklearn.preprocessing import StandardScaler
from sklearn.cluster import KMeans

# Extract the relevant features
X = df[['Colocalization Index', 'UPSIT Score', 'Radioactivity (nCi-kg/cc-mCi)']].values

# Normalize the features
scaler = StandardScaler()
X_normalized = scaler.fit_transform(X)

# Perform K-Means clustering on the normalized data
kmeans = KMeans(n_clusters=2, random_state=0, n_init=10).fit(X_normalized)

# Add the cluster labels to the original DataFrame
df['Cluster'] = kmeans.labels_

# Inverse transform the centroids to original scale
centroids_original_scale = scaler.inverse_transform(kmeans.cluster_centers_)

# Plot the data and the centroids
fig = go.Figure()
```

```
896
897     # Add the data points for cluster 0
898     fig.add_trace(go.Scatter3d(
899         x=df[df['Cluster'] == 0]['Colocalization Index'],
900         y=df[df['Cluster'] == 0]['UPSIT Score'],
901         z=df[df['Cluster'] == 0]['Radioactivity (nCi-kg/cc-mCi)'],
902         mode='markers',
903         marker=dict(size=5, color='red',symbol='circle'),
904         name='Cluster 0'
905     ))
906
907     # Add the data points for cluster 1
908     fig.add_trace(go.Scatter3d(
909         x=df[df['Cluster'] == 1]['Colocalization Index'],
910         y=df[df['Cluster'] == 1]['UPSIT Score'],
911         z=df[df['Cluster'] == 1]['Radioactivity (nCi-kg/cc-mCi)'],
912         mode='markers',
913         marker=dict(size=6, color='red',symbol='circle'),
914         name='Cluster 1'
915     ))
916
917     # Add the centroids (transformed back to the original scale)
918     fig.add_trace(go.Scatter3d(
919         x=centroids_original_scale[:, 0],
920         y=centroids_original_scale[:, 1],
921         z=centroids_original_scale[:, 2],
922         mode='markers',
923         marker=dict(size=10, color='green', symbol='diamond'),
924         name='Centroids'
925     ))
926
927     # Update the layout for a clearer view
928     fig.update_layout(
929         scene=dict(
930             xaxis_title='Colocalization Index',
931             yaxis_title='UPSIT Score',
932             zaxis_title='Radioactivity (nCi-kg/cc-mCi)'
933         ),
934         width=800,  # Set the width of the plot
935         height=800,  # Set the height of the plot
936     )
937
938     # Show the figure
939     fig.show()
940
941
```

Supplementary Files

This is a list of supplementary files associated with this preprint. Click to download.

- STROBEChecklist.docx
- SupplementaryWorkbook18FDAUPSITColoc.LBnOHData.xlsx